DR MATTEO BALLOTTARI (Orcid ID : 0000-0001-8410-3397)

Article type : Original Article

LPA2 protein is involved in Photosystem II assembly in *Chlamydomonas reinhardtii*

Michela Cecchin[1*], Jooyeon Jeong[2*], Woojae Son[3*], Minjae Kim[2], Seunghye Park[2], Luca Zuliani[1], Stefano Cazzaniga[1], Andrea Pompa[4, 5], Chan Young Kang[3], Sangsu Bae[3], Matteo Ballottari[1#], EonSeon Jin[2#]

[1] Dipartimento di Biotecnologie, Università di Verona, Verona, Italy

[2] Department of Life Science, Hanyang University, Seoul, Korea

[3]Department of Chemistry, Hanyang University, Seoul, Korea

[4]Dipartimento di Scienze Biomolecolari, Università degli studi di Urbino

[5] Istituto di Bioscienze e Biorisorse, Consiglio Nazionale delle Ricerche, Perugia, Italy

* MC, JJ, and WS contributed equally to this work

[#] Corresponding authors

Running title: The role of LPA2 in PSII assembly in green algae

This article has been accepted for publication and undergone full peer review but has not been through the copyediting, typesetting, pagination and proofreading process, which may lead to differences between this version and the Version of Record. Please cite this article as doi: 10.1111/TPJ.15405

Keywords: Photosystem II, Chlamydomonas reinhardtii, Photosynthesis, Chloroplast biogenesis, Genome editing, CRISPR

Corresponding authors details:

EonSeon Jin, Department of Life Science, Research Institute for Natural Sciences, Hanyang University, 222, Wangsimni-ro, Seongdong-gu, Seoul, 04763, Korea. E-mail: esjin@hanyang.ac.kr;

Matteo Ballottari, Dipartimento di Biotecnologie, Università di Verona, Strada le Grazie 15, Verona, Italy. E-mail: matteo.ballottari@univr.it

SUMMARY

Photosynthetic eukaryotes require the proper assembly of photosystem II (PSII) to strip electrons from water and fuel the carbon fixation reactions. In *Arabidopsis thaliana*, one of the PSII subunits (CP43/PsbC) was suggested to be assembled into the PSII complex via its interaction with an auxiliary protein called Low PSII Accumulation 2 (LPA2). However, the original articles describing the role of LPA2 in PSII assembly have been retracted. To investigate the function of LPA2, here we generated in the model organism for green algae, *Chlamydomonas reinhardtii,* knockout *lpa2* mutants by using the CRISPR-Cas9 target-specific genome-editing system. Biochemical analyses revealed the thylakoidal localization of LPA2 protein in the WT while *lpa2* mutants were characterized by a drastic reduction in the level of D1, D2, CP47 and CP43 proteins. Consequently, reduced PSII supercomplex accumulation, chlorophyll content per cell, PSII quantum yield and photosynthetic oxygen evolution were measured in the *lpa2* mutants, leading to an almost complete impairment of photoautotrophic growth. Pulse-chase experiments demonstrated that the absence of LPA2 protein caused a reduced PSII assembly and reduced PSII turnover. Taken together, our data indicate that, in *C. reinhardtii*, LPA2 is required for PSII assembly and its proper function.

INTRODUCTION

Photosystem II (PSII) is the initial complex in the linear electron transport of photosynthesis in chloroplasts (Nelson and Junge, 2015). It comprises the light-harvesting antenna complex that absorbs sunlight and the core complex that converts light into photochemical energy (van Amerongen and Croce, 2013, Su *et al.*, 2017, Shen *et al.*, 2019) The PSII core complex contains at least 20 subunits with various cofactors, including electron donors and acceptors (Gokhale and Sayre, 2009). Because of the structural complexity of PSII, the proper assembly of its subunits is important for its function (Nickelsen and Rengstl, 2013, Lu, 2016).

Although photosynthetic eukaryotes have, through endosymbiosis, acquired chloroplasts that perform oxygenic photosynthesis, the chloroplast genome does not encode all the proteins necessary for the photosynthetic machinery (Shinozaki *et al.*, 1986). Numerous nuclear genes encode components of the photosynthetic apparatus. Moreover, multiple proteins required for the biogenesis and assembly of protein complexes in the chloroplast, e.g., the CpSRP54, CpSRP43, CpFTSY, and LTD proteins from the chloroplast signal recognition particle pathway, are encoded by nuclear genes (Kirst and Melis, 2014, Jeong *et al.*, 2017, Ziehe *et al.*, 2017, Jeong *et al.*, 2018).

The biogenesis of PSII is a step-wise assembly process (Nickelsen and Rengstl, 2013, Lu, 2016). The first step is the formation of the D1 and D2 heterodimer, where the chlorophyll special pair involved in PSII photochemistry is bound (Rokka *et al.*, 2005). Next, the inner antenna proteins CP47 and CP43 are sequentially bound (Boehm *et al.*, 2011). Subsequently, the oxygen-evolving complex assembles on the lumenal side of the PSII pre-complex, which is converted into an active monomeric PSII (Rokka *et al.*, 2005, Bricker *et al.*, 2012). Finally, the active PSII forms dimers and is surrounded by the peripheral light-harvesting antenna complex, which completes the *de novo* biogenesis of PSII (Nickelsen and Rengstl, 2013, Su *et al.*, 2017, Shen *et al.*, 2019).

Many regulatory factors are involved in the appropriate organization of the PSII subunits. Of these, Psb27 in cyanobacteria interacts with CP43 and PSII during both *de novo* biogenesis and repair of PSII (Komenda *et al.*, 2012). Because two Psb27 homologs have been identified in the green lineage, the role of cyanobacterial Psb27 was proposed to be divided between two genes in eukaryotes (Nickelsen and Rengstl, 2013). One of them, Psb27-H2 (LPA19), participates in *de novo* PSII assembly by interacting with D1 and CP43 (Wei *et al.*, 2010).

In cyanobacteria, CP43 incorporation into PSII requires another assembly factor, Sll0606, whose absence results in a drastic reduction in the level of PSII (Zhang *et al.*, 2010). A homolog of

Sll0606 is found in the microalga *Chlamydomonas reinhardtii*, but not in the land plant *Arabidopsis thaliana*, suggesting that Sll0606 might be functionally replaced by other proteins in embryophytes (Chi *et al.*, 2012, Nickelsen and Rengstl, 2013). One possible replacement is low PSII accumulation 2 (LPA2), which has been suggested to interact with CP43 during PSII assembly in *A. thaliana*, although based on reports that have been retracted (Ma *et al.*, 2007, Cai *et al.*, 2010). A reduced PSII activity and reduced growth was also reported in *A. thaliana lpa2* mutants in a following work, where LPA2 was shown to interact with TerC (Tellurite resistance C) protein, involved in insertion of thylakoid membrane proteins (Schneider *et al.*, 2014). LPA2 homologs have been found in other embryophytes, but not in *C. reinhardtii* or cyanobacteria (Chi *et al.*, 2012, Nickelsen and Rengstl, 2013). Therefore, CP43 assembly was not expected to require an LPA2 homolog in *C. reinhardtii*, but no detailed study of the assembly factors for CP43 in this microalga has been performed. In this study, we identified an LPA2 homolog in the *C. reinhardtii* genome. To investigate the function of this protein *in vivo*, we used the ribonucleoprotein (RNP)-mediated CRISPR-Cas9 system to generate target-specific knockout mutants (*lpa2*) of *C. reinhardtii*. In the absence of the LPA2 protein, *lpa2* mutants had reduced amount of PSII core subunits and dysfunctional PSII supercomplexes. These results indicate that LPA2 is required for efficient PSII assembly in *C. reinhardtii*. In addition, *lpa2* mutants had enhanced electron transport around PSI, suggesting that PSI can be used to dissipate excitation energy in PSII-deficient conditions.

RESULTS

LPA2 gene in *C. reinhardtii*

The putative *LPA2* gene (Cre02.g105650) was identified in the *C. reinhardtii* genome based on the amino acid sequence similarity between its product and LPA2 in *A. thaliana* (Figure 1). Homologs were also identified in the green lineage, including chlorophytes, but not in cyanobacteria. Moreover, no LPA2 homologs could be found in *Glaucophytes, Rhodophyta* or in species derived from secondary endosymbiosis as *Cryptophyta, Haptophyta*, or *Heterokonta* suggesting that the LPA2 protein is of eukaryotic origin, being evolved in particular in *Viridiplantae* (Table S1, Figure 1A). *LPA2* gene could be identified also in bryophytes, lycophytes and tracheophytes but not in hornwort, where no homolog could be found. The absence of LPA2 gene in hornwort could be related to some specific evolutive events that require a dedicated and in-depth analysis. The *C.*

reinhardtii LPA2 gene (*CrLPA2*) encodes a protein of 175 amino acids, including a 24 amino-acid-long chloroplast transit peptide predicted by Predalgo software (https://giavap-genomes.ibpc.fr/predalgo/) and two transmembrane domains (amino acids 109–131 and 146–163) determined by TMHMM software (http://www.cbs.dtu.dk/services/TMHMM/). The CrLPA2 protein shares 23.2% identity and 43.2% similarity with its *Arabidopsis* homolog (Figure 1B).

To investigate the function of *C. reinhardtii* LPA2, we analyzed the light-inducible expression of *LPA2*. We exposed *C. reinhardtii* strain CC503 to high light (500 μmol photons m^{-2} s^{-1}) for 0, 30, and 60 min and used qRT-PCR to analyze the transcript levels of *ELIP2* and *LPA2* (Supporting Information Figure S1A). While in the case of *ELIP2* high light treatment caused a statistically significant increased transcription, *LPA2* expression was only moderately enhanced after exposure to high light. Western blotting revealed the presence of LPA2 in purified chloroplasts, specifically in the thylakoid membranes, but not in the stromal fraction (Supporting Information Figure S1B).

Generation of knock-out mutants without the *LPA2* gene in *C. reinhardtii*

To further characterize *C. reinhardtii* LPA2, we generated target-specific knockout mutants by using preassembled Cas9 protein–small guide RNA (sgRNA) RNP complex–mediated CRISPR-Cas9. Different sgRNA were tested for the generation of *lpa2* mutants with positive results obtained only in the case of sgRNA2 containing the 5′-CAAGGGCTTTGGTTCAGAGACGG-3′ sequence (Table S2). Considering a possible phenotype on the assembly of the pigment binding complexes (Ma *et al.*, 2007), *lpa2* mutant strains were screened on the basis of Chl fluorescence. Transformants with lower F_v/F_m fluorescence signals than the background cells (Figure 2A) were selected for Sanger sequencing analysis of the target locus. All such transformants had small indels in the *LPA2* gene (Figure 2B). The knock-out efficiency, calculated as the ratio of the mutant number (3) to the total colony number (606), was 0.495%, which was similar to the targeted mutation frequency obtained from the total gDNA of CRISPR-Cas9–transfected cells (0.4%; Table S3). Transcription of *LPA2* gene was investigated in the *lpa2* mutants compared to the WT case revealing a reduced transcription in the mutants (Figure 2C). Cas9 driven mutations occurred at the first exon of *LPA2* gene, where *lpa2#1* and *lpa2#2* mutants were deleted by 2bp and 5bp, respectively (Figure 2B): we can speculate that these deletions may cause non-functional transcripts that could be unstable in mutants, as previously reported for other genes edited by Cas9 (Tang *et al.*, 2018, Tuladhar *et al.*, 2019), even if further work is required to support this hypothesis. LPA2 protein accumulation was then investigated by immunoblotting analysis

showing no detectable results in the case of *lpa2* mutant strains (Figure 2D). Analysis of the *lpa2* mutants for potential off-target effects by targeted deep sequencing revealed no indels (Table S4).

Decreased chlorophyll (Chl) content in the *lpa2* mutants

As revealed during mutant screening, *lpa2* mutants had an aberrant F_v/F_m fluorescence signal (Figure 2E). Interestingly, although the F_m/Chl ratios of the mutants were similar to that of the wild type, the F_0/Chl ratios of the mutants were increased, resulting in a low F_v/F_m fluorescence signal. The increased F_0/Chl ratio suggests the partial disconnection of antenna complexes from PSII. The organization of the photosynthetic apparatus was thus investigated on the basis of 77K fluorescence emission spectra. In the case of *lpa2* mutants, the spectra were characterized by an increased fluorescence emission at 680 nm which can be ascribed to the presence of a disconnected LHC protein, confirming the partial destabilization of the PSII complexes (Supporting Information Figure S2). Interestingly, *lpa2* mutants were characterized by an increased 715/686 nm and 715/690 fluorescence emission ratios. 686 and 690 nm fluorescence emission are related to PSII contributions, while 715 nm is due to PSI emission (Snellenburg *et al.*, 2017, Girolomoni *et al.*, 2019): increased 715/686 nm or 715/690 nm fluorescence emission ratios in *lpa2* mutants compared to the WT case suggests an increased PSI/PSII ratio and/or increased antenna proteins bound to PSI in the mutant strains.

To understand the change in Chl fluorescence caused by the mutation, we analyzed the Chl content of the *lpa2* mutants (Table 1). In photoautotrophic cultures, *lpa2* mutants exhibited approximately 50% reduction in total Chl content per cell compared with that in the wild type, whereas the Chl *a*/*b* ratio were not significantly affected. The reduction in Chl content per cell was not related to a change in cell size, which was similar in the different strains analyzed (Table 1).

***lpa2* mutants had strongly reduced photoautotrophic growth and reduced photosynthetic activity**

To investigate how the reduced Fv/Fm and reduced chlorophyll content found in the *lpa2* mutants affected their growth, we cultivated wild-type (WT) and mutant strains under photoautotrophic, mixotrophic, and heterotrophic conditions. Under heterotrophic conditions (with acetate as a source of organic carbon), the growth of *lpa2* mutants was similar to that of WT, indicating that the mutations introduced did not affect the light-independent cell functions. In mixotrophy, *lpa2* mutants showed slower growth than the WT in both solid and liquid media. Under

photoautotrophic conditions, the growth of *lpa2* mutants was severely impaired (Figure 3), presumably because the lower photosynthetic activity of the mutants could not maintain whole-cell metabolism under these conditions. Interestingly, in the case of lpa2 mutants the doubling time at exponential phase were similar in mixotrophy and heterotrophic conditions, suggesting that the growth rate in TAP medium was essentially driven by acetate consumption in this mutant strains (Table 2). Consistently, *lpa2* mutants were essentially not replicating in the time range analyzed in photoautotrophic growth conditions. Differently, WT cells grown in mixotrophy were characterized by a reduced doubling time compared to both heterotrophic and photoautotrophic conditions. The photosynthetic activity of *lpa2* mutants was then analyzed using pulse-amplitude-modulated (PAM) fluorescence (Supporting Information Figure S3). The operating efficiency of PSII electron transport (ΦPSII) was lower in the mutants than in the WT at light intensities below 400 μmol $m^{-2}s^{-1}$, but similar at higher irradiances (Supporting Information Figure S3). The fraction of excitation energy not used for the photochemical reaction could be lost through safe non-photochemical reactions leading to controlled energy conversion into heat (ΦNPQ) or through uncontrolled dissipation (ΦNO), which is usually related to oxidative stress and photoinhibition. Controlled thermal dissipation of the absorbed excitation energy (ΦNPQ) was also lower in the *lpa2* mutants than in the WT, whereas the fraction of absorbed energy lost by uncontrolled dissipation (ΦNO) was higher in *lpa2* (Supporting Information Figure S3A,B and C). Accordingly, the NPQ values, calculated as (Fm-Fm′)/Fm′, were lower in the *lpa2* mutants than in the WT, implying a lower photoprotective capacity in the mutants (Supporting Information Figure S3E and F). The fraction of closed PSII centers, calculated from the 1 - q_L value, was similar in the *lpa2* mutants compared to that in WT (Supporting Information Figure S3E). This result indicates that, despite the reduced efficiency of PSII, the redox state of Q_A was maintained similar to that in the WT at the different light intensities owing to an acclimation of the overall photosynthetic apparatus. We further investigated PSII activity by measuring the light-dependent oxygen evolution curves and found reduced oxygen evolution on a per-cell basis in the *lpa2* mutants, confirming its reduced photosynthetic activity (Figure 4A).. In order to investigate specifically the PSII activity, oxygen evolution was measured in presence of electron acceptor for plastoquinones as 2,6-Dichloro-1,4-benzoquinone (DCBQ) and its the secondary acceptor potassium ferricyanide (III), in presence of inhibitor DBMIB, preventing possible influence of PSI on plastoquinone redox state (Böhme, 1976, Brinkert *et al.*, 2016). As reported in Figure 4C reduced PSII activity was measured in presence of DCBQ, potassium ferricyanide (III) and

DBMIB in *lpa2* mutants. Interestingly, in presence of electron acceptor for plastoquinones, light dependent net oxygen evolution was linearly correlated with the level of D1 or D2 (Figure 4D). This result suggests that the lower oxygen evolution was due to decreased PSII accumulation in the mutants..

The *lpa2* mutants have enhanced electron transport flow around PSI

PSI activity was measured as maximum P700 oxidation, which was higher on a Chl basis in the *lpa2* mutants than in the wild type (Figure 5A), but similar on a per cell basis because of the reduced Chl content per cell in the mutants (Figure 5B). These results suggest that the defect in PSII activity increased PSI activity on a chlorophyll basis in the *lpa2* mutants.

Next, we measured the electrochromic shift (ECS) to estimate the proton-motive force (*pmf*) across the thylakoid membranes generated by the light-driven electron flux. The *pmf* in the *lpa2* was similar to that in the WT (Figure 5C). Considering the reduced PSII activity in the *lpa2* mutants, we investigated the possible influence on cyclic electron flow (CEF) around PSI on *pmf* by measuring the ECS in the presence of DCMU to inhibit linear electron flow. The *lpa2* mutants had an increased fraction of *pmf* related to CEF (Figure 5C), causing a similar total *pmf* despite decreased PSII activity.

We reasoned that the altered amounts PSII activity in the *lpa2* mutants might affect the state transitions that balance the energy between PSI and PSII by using LHCII migration from PSII to PSI. We examined the capacity of the *lpa2* mutants to perform state transitions by measuring the 77K fluorescence emission spectra of cells under state 1 or state 2 conditions (Figure 5D, E and F). The *lpa2* mutants showed increased migration of light-harvesting antenna proteins to PSI under state 2 conditions, suggesting an increased pool of mobile LHCII subunits, likely because of the reduced PSII assembly.

The *lpa2* mutants accumulate low amount of PSII core subunits

We investigated the effect of the *LPA2* gene mutation on the organization of photosynthetic complexes in isolated thylakoid membranes (Figure 6). In the 2D-Deriphat/SDS-PAGE analysis, the intensity of the bands representing the PSII core and PSII supercomplexes was markedly reduced in the *lpa2* mutant, with a particularly strong decrease in the CP43/CP47 band and, even if to lower extent, D1/D2 band. Interestingly, LPA2 protein was detected in the WT as a monomer and at higher oligomerization state, likely interacting with other proteins involved in PSII

assembly, as previously reported in the case of *A. thaliana* (Ma *et al.*, 2007, Schneider *et al.*, 2014).

Western blot analyses of specific photosystem subunits (Figure 7), revealing, on a chlorophyll basis, the strongest decrease in CP43, with ~20% residual CP43 in the *lpa2* mutants, followed by CP47, D1 and D2 which were reduced to ~30-40% compared to the WT case. Significant reduced accumulation of other PSII core subunits as PsbO and PsbP was also detected in the case of *lpa2* mutants (Figure 7). The accumulation of LHCII complexes in the *lpa2* mutants was similar to that in the WT on a chlorophyll basis, indicating that the LHCII/PSII ratio in the mutants was increased. Considering the low NPQ measured in the case of *lpa2* mutants, the accumulation of LHCSR3, the main chlorophyll binding protein involved in this photoprotective mechanism was also investigated (Peers *et al.*, 2009). As reported in Figure 7, a ~50% reduction of LHCSR3 was measured on chlorophyll basis in the absence of LPA2. LHCSR proteins have been reported to be involved in quenching mechanisms occurring both at the level of PSII, disconnected LHCII and PSI-LHCI (Dinc *et al.*, 2016, Girolomoni *et al.*, 2019, Cazzaniga *et al.*, 2020): while in the ratio LHCSR3/PSII was similar in WT and *lpa2* mutants, a reduced LHCSR3/LHCII and LHCSR3/PSI was evident in the latter.

PSI accumulation on a chlorophyll basis was not affected by the *LPA2* mutation (Figure 7), with a consequent increase in the PSI/PSII ratio in the *lpa2* mutants compared with that in the WT. Interestingly, in the case of LHCI a possible reorganization of different Lhca subunit likely occurred in *lpa2* mutants, as evinced by the different content of subunits recognized by α-Lhca3 and α-Lhca4 antibodies in the *lpa2* mutants, which were respectively decreased and increased on a chlorophyll basis compared to the WT case.. It has already been reported that the quality of the Lhca complexes bound by PSI can be modulated according to the different growth conditions (Bonente *et al.*, 2012): the destabilization of PSII observed in *lpa2* is thus likely inducing acclimation mechanisms at the level of PSI.

The accumulation of the cytochrome b_6f complex and ATP synthase was investigated using western blotting by using antibodies specific to cytochrome *f* and the ATPase β-subunit, respectively (Figure 7). The levels of both subunits were significantly increased on a chlorophyll basis in the *lpa2* mutant. The large Rubisco subunit, a representative enzyme of the Calvin–Benson cycle, was clearly increased in the mutants on a chlorophyll basis. As reported in Figure 7D the reduced PSII content on a chlorophyll basis was accompanied in *lpa2* mutants by a strong increase of cytochrome b_6f complex, PSI, Rubisco, and ATP synthase content per PSII. On a cell

basis, due to the reduce chlorophyll content observed in the case of *lpa2* mutants, the strong decrease in PSII subunits in these strains was accompanied by a reduction of PSI and cytochrome b_6f complex, and a similar content of Rubisco and ATP synthase compared to the WT case (Supporting Information Figure S4)..

In order to evaluate if the absence of LPA2 protein specifically affected PSII assembly or its turnover rate, we performed pulse-chase experiments, followed by thylakoid solubilization and PSII core immunoprecipitation by using D2 antibodies. As reported in Figure 7E, upon SDS-PAGE separation of proteins co-immunoprecipitated by D2 antibody, two main bands respectively at ~45 kDa and ~35 kDa were appearing: the former can be attributed to CP43 and/or CP47, while the latter to D2, likely with the comigration of the subunit D1 (Figure 7F). The *lpa2* mutants were characterized by similar incorporation of D1/D2 and in PSII complex compared to WT in time range herein analyzed. Differently, a strongly reduced CP43/CP47 assembly was evident after a 60- or 120-minutes pulse F, suggesting the key role of LPA2 in PSII assembly. After 1 hour of chase in low light, the D1/D2 and CP47 contents were strongly reduced in the case of WT because of its high turnover rate and assembly of new label-free complexes, but not in the *lpa2* mutants, indicating a slower PSII turnover, likely as a consequence of the partially impaired assembly.

PSII photosensitivity and D1 repair in *lpa2* mutants

PSII complexes which are not fully assembled are highly unstable and more sensitive to high light treatment, which causes photooxidation (Fu *et al.*, 2007). We monitored the level of D1 protein during high light (500 μmol m^{-2} s^{-1}), exposure in the presence or absence of lincomycin, a chloroplast protein biosynthesis inhibitor (Supporting Information Figure S5). In the *lpa2* mutant, the relative level of D1 protein decreased faster than in the WT when they were shifted from low light to high light, suggesting an increased photosensitivity of PSII complexes in the mutants. To explore the photosensitivity of PSII in *lpa2* mutants and the potential role of the LPA2 protein in repairing D1 subunit, we performed light shift experiments and monitored the rate of photoinhibition and recovery. After exposure to strong light (1800 μmol m^{-2} s^{-1}), the Fv/Fm values were remarkably reduced in *lpa2* mutants (Figure 8A), with a considerably faster rate than that of the WT, suggesting a strong photosensitivity in the absence of the LPA2 protein. Upon shift to low light (15 μmol m^{-2} s^{-1}), PSII repair mechanisms were activated: the PSII repair occurred faster in the *lpa2* mutants (Figure 8B). On a longer time, PSII repair in the WT was more effective, leading to the restoration of higher Fv/Fm values than those in *lpa2* mutants. These

results are consistent with the reduced CP43/CP47 incorporation in PSII complexes resulting in pulse experiments at longer time scale (60- or 120-minutes pulses).

DISCUSSION

Here, we demonstrate that differently from previous report (Ma *et al.*, 2007), a LPA2 homolog is present in the model organism for green algae *C. reinhardtii*. Moreover, we found LPA2 homologs in different *Chlorophytes*, but not in cyanobacteria, or in other eukaryotic algae species, suggesting that LPA2 evolved specifically in eukaryotes belonging to the green lineage. Therefore, to expand our understanding of PSII biogenesis and assembly in green algae, we used the CRISPR-Cas9 methodology to investigate this nuclear-encoded protein, LPA2, and elucidate its role in PSII biogenesis via photochemical and biochemical analysis of two independent *lpa2* mutants.

Lack of LPA2 affects PSII assembly in *Chlamydomonas reinhardtii*

The lack of the LPA2 protein, which is localized in the thylakoid membranes, resulted in a strong reduction of the growth of *lpa2* mutants in mixotrophy condition and an almost complete impairment of growth in photoautotrophy (Figure 3). Similar results were previously obtained in *C. reinhardtii* mutants depleted of CP43 (Zerges *et al.*, 2003, Marín-Navarro *et al.*, 2007): in the case of *lpa2* mutants CP43 subunit was observed reduced to ~20% of the WT level. In the absence of LPA2 protein, other PSII core subunits were also decreased, with ~60-70% reduced accumulation of CP47, D1 and D2 being lost on a chlorophyll basis in *lpa2* mutants (Figure 7). Pulse-chase experiments showed that, in the absence of LPA2, the assembly of D1/D2 complexes into PSII occurs to similar rate compared to WT. Differently, in the case of CP43/CP47, their assembly into PSII was essentially saturated in *lpa2* mutants in the first 30 minutes while further increased in the WT even after 120 minutes pulse (Figure 7E). The thylakoidal LPA2 protein is thus involved in the assembly of CP43/CP47 to PSII, which also contributes to the stabilization of the overall PSII core complex. It is worth to mention that PSII assembly proceed through the formation of D1/D2/CP47 complex with a following incorporation of CP43: LPA2 could be specifically involved in the assembly of CP43 to PSII, as previously suggested in *A. thaliana* by the retracted work of Ma and coworker (Ma *et al.*, 2007). Alternatively, LPA2 could be involved

in both CP43 and CP47 assembly to PSII: additional research efforts are required to discriminate between these two different hypotheses.

PSII in t3Dhe *lpa2* mutants showed increased photosensitivity (Figure 8 and Supporting Information Figure S5) at high light intensity. D1 is the PSII component that is the most sensitive to excess light energy (Melis, 1999, Nickelsen and Rengstl, 2013); photodamaged D1 is rapidly replaced with newly synthesized D1 (Nickelsen and Rengstl, 2013, Järvi *et al.*, 2015, Lu, 2016). For D1 replacement, PSII is partially disassembled by the detachment and reassembly of CP43 (Nickelsen and Rengstl, 2013, Järvi *et al.*, 2015, Lu, 2016). Previous works demonstrated that in *C. reinhardtii* de novo PSII assembly and D1 repair are distinct mechanisms occurring in different regions of the chloroplast (Uniacke and Zerges, 2007). Indeed, despite a slower PSII turnover rate observed in the case of *lpa2* mutants during chase experiments, D1 repair was enhanced in the shorter time scale in the mutants upon strong light exposure (Figure 8). Faster recovery of PSII activity in *lpa2* mutants (Figure 8B) could be related to increased activation of D1 repair mechanism as an acclimation response due to increased photosensitivity of the partially assembled PSII complexes occurring in the absence of LPA2 protein. In *A. thaliana*, LPA3 is a major factor required for CP43 detachment during D1 repair; no evidence suggests that LPA2 is involved in PSII repair (Chi *et al.*, 2012, Järvi *et al.*, 2015). Our D1 regeneration results in *C. reinhardtii lpa2* mutants indicate that indeed the involvement of LPA2 in PSII repair is limited and related to longer time scale, while the main role of this protein is occurring in *de novo* biogenesis of PSII.

Lack of LPA2 affects the accumulation of the photosynthetic machinery

The absence of the LPA2 protein increased the F_0/Chl ratio and caused an increased contribution of the 77 K fluorescence emission spectra at 680 nm in the *lpa2* mutant, indicating that the efficiency of excitation energy transfer from the antenna complex to the reaction center is reduced because of the partial disconnection of the PSII-LHCII supercomplex (Figure 2E, Supporting Information Figure S2). Likewise, native Deriphat-PAGE showed a lower level of the PSII-LHCII supercomplex in the mutant, if any, but the unconnected LHCII remained as a free antenna (Figure 6). A large decrease in CP43 and CP47 in the mutants implies that *C. reinhardtii* LPA2 participates in their accumulation, as these subunits are an important link between the PSII reaction center and the antenna complex. The reduced PSII assembly in *lpa2* mutants caused a reduction of PSII activity (Figure 4), which contributed to the reduced growth phenotype observed in the *lpa2* mutants (Figure 3), which became even more severe under photoautotrophic conditions

causing the whole-cell metabolism to rely on photosynthesis. The increase in the ΦNO of the mutants also indicated insufficient photoprotective regulation of energy dissipation (Supporting Information Figure S3), in agreement with the increased photosensitivity of PSII in these mutants and posing a serious problem for *lpa2* mutants survival without a carbon source (Figure 3). One of the main photoprotective mechanism in green algae, NPQ was reduced in *lpa2* mutants, despite the trigger for this mechanism, protons accumulation in the lumen (Peers *et al.*, 2009), was similar compared to WT, as resulting from ECS measurements (Figure 5C). Accordingly, LHCSR3 content was reduced in the absence of LPA2 protein (Figure 7), but the ratio between LHCSR3 and PSII was similar in WT and *lpa2* mutants. However, it is worth to note that LHCSR proteins has been reported to functions as a quencher also at the level of disconnected LHCII (Dinc *et al.*, 2016) and PSI-LHCI antenna (Kosuge *et al.*, 2018, Girolomoni *et al.*, 2019), with LHCSR3/LHCII and LHCS3/PSI ratios being reduced in the *lpa2* mutants (Figure 7). Moreover, LHCSR3 expression and maximum NPQ activity should be investigated in high light, while *lpa2* mutants presented a reduced growth phenotype even at low light (Peers *et al.*, 2009): further work are required to investigate more deeply the reason for the low NPQ phenotype of *lpa2* mutants. Another mechanism previously reported to be involved in photoprotection of *C. reinhardtii* is the migration of balance of excitation pressure among PSI and PSII by state transitions (Allorent *et al.*, 2013). The increase state transition capacity of *lpa2* mutants could be a consequence of the reduced PSII activity, inducing a migration of antenna proteins toward PSI. Alternatively, the reduced PSII-LHCII supercomplex formation might cause and increased fraction of mobile LHCII, resulting in increased state transitions capacity.

Unlike PSII, the abundance of PSI core subunits and PSI activity were not reduced by the lack of LPA2 protein (Figure 7, Figure 5) with a consequent increase of the PSI/PSII ratio in the mutant. These findings differ from those of previous studies showing lower PSI activity in mutants defective in PSII biogenesis (Zhang *et al.*, 2011, Wang *et al.*, 2013), including the case of *lpa2* mutants in *A. thaliana* (Ma et al., 2007). These features suggest that in *C. reinhardtii* the *lpa2* mutants might preferentially operate PSI-mediated electron transport flow to release excitation pressure and generate trans-thylakoid proton transport to compensate for the inactive PSII. Indeed, the fraction of CEF, which is critical in maintaining the *pmf*, was higher in the *lpa2* mutants than in the WT (Figure 5).

The imbalance between PSII and PSI in the *lpa2* mutants resulted in another interesting phenotype: over accumulation on a chlorophyll basis of the cytochrome b_6f complex and Rubisco,

which are involved in down-stream photosynthetic reactions (Figure 7D). Similarly, ATP synthase content was increased in *lpa2* mutants, suggesting a possible faster relaxation of lumen acidification. However, the observed reorganization of the photosynthetic apparatus in the *lpa2* mutants is not sufficient to sustain photoautotrophic growth, likely because of the reduced PSII dependent linear electron flow, causing a consequent reduced NADPH formation and increased photosensitivity.

Comparison between LPA2 functions in *Chlamydomonas reinhardtii* and *Arabidopsis thaliana*

Comparing the effect of *lpa2* mutation in *C. reinhardtii* with the previous retracted results reported in the *A. thaliana* (Ma *et al.*, 2007), several features were shared, as severely reduced growth, reduced PSII assembly, strong reduction in PSII core subunits accumulation, reduced PSII activity and photochemical efficiency, and increase in Cyt *f* content and ATPase (Ma *et al.*, 2007). However, in the case of *C. reinhardtii* an increase PSI/PSII ratio and increased P700 activity on a chlorophyll basis were evident in the *lpa2* mutant, while in *A. thaliana* both PSI accumulation and P700 activity were lower compared to the WT case. In the absence of LPA2 protein causing reduced PSII assembly, the cell acclimation mechanisms were thus partially different in *C. reinhardtii* compared to *A. thaliana*, with a specific increase in PSI activity in the former. Moreover, here we report increased RUBISCO content, increased state transitions, increased CEF, increased D1 repair but reduced NPQ capacity in *C. reinhardtii* in *lpa2* mutants, while similar acclimation events in the case of *A. thaliana lpa2* mutants were not investigated up to now, to our knowledge.

In conclusion, the knockout mutation of *LPA2* in *C. reinhardtii* resulted in a drastic reduction in the level of PSII, with a concomitant decrease in its efficiency. In the absence of the thylakoidal LPA2 protein, not only the accumulation of CP43/CP47/D1/D2 were strongly reduced, but residual PSII was more prone to photoinhibition leading to increased D1 repair on a short time scale. However, further studies are required to understand the detailed mechanism by which LPA2 plays that role. The process of PSII protein assembly is complicated, and the functions of various assembly factors are almost certainly coordinated. Some of these factors such as LPA1/rep27, PAM68, and Alb3, which function in the same step, could form a protein complex (Armbruster *et al.*, 2010); thus, building a protein interaction network that can provide a comprehensive view of

the interplay among different assembly factors, repair complexes, and PSII subunits is necessary. PSII assembly factors such as Alb3 and PAM68 emerged early in the evolution of photosynthetic organisms because they are present in all cyanobacterial groups, green algae, and embryophytes (Chi *et al.*, 2012). Conversely, LPA2 is present in the green lineage (Figure 1), but no homolog of LPA2 has been identified in the cyanobacterium *Synechocystis* PCC6803, red algae, glaucophytes, and algae that contain a red algal plastid, suggesting that LPA2 appeared in the green plant lineage (Chi *et al.*, 2012).

It is worth to note that during the revision process of this work, a preprint was released reporting a role of LPA2 in PSII assembly in *C. reinhardtii*, essentially confirming the results herein described (Spaniol *et al.*, 2021).

EXPERIMENTAL PROCEDURES

Sequence alignments and phylogenetic analysis

LPA2 homologs were identified in the NCBI non-redundant protein sequences database using BlastP. The obtained sequences showed a Blast query coverage more than 50 % of the alignment and at least 40 % amino acid identity to LPA2 of *A. thaliana* or *C. reinhardtii*. Additionally, we searched more homolog sequences in the DOE-JGI Phytozome proteome database using Blast and selected sequences that matched the HMM profile with an e value < 10^{-3} (Potter *et al.*, 2018). The species and accession numbers of LPA2 homologs were summarized in Table S1. LPA2 homolog was not found in Glaucocystophyceae, Rhodophyta, Cryptophyceae, Haptista, Rhizaria, Stramenopiles and Alveolata. The amino acid sequences were aligned using MUSCLE with the default settings of Geneious R10 software (Edgar, 2004) and the non-conserved regions of the alignment were trimmed manually using Mesquite software Version 3.61 (http://www.mesquiteproject.org). Maximum likelihood tree was constructed using PhyML3 with 100 bootstrap analysis (Guindon *et al.*, 2010). The WAG substitution model was selected assuming an estimated proportion of invariant sites and four gamma-distributed rate categories by SMS (Whelan and Goldman, 2001, Lefort *et al.*, 2017). The obtained tree was visualized and edited using Archaeopteryx (http://www.phylosoft.org/archaeopteryx).

CRISPR-Cas9-driven mutagenesis

All procedures were performed according to (Baek *et al.*, 2016) by using 100 μg of Cas9 protein and 70 μg of gRNA. After CRISPR-Cas9 transformation, cells were incubated in TAP liquid medium supplemented with 40 mM sucrose for 12 h and harvested for genotype characterization or immediately diluted (to 2×10^3 cells) and plated on TAP medium containing 1.5% agar to obtain single colonies. The colonies were screened on the basis of the F_v/F_m fluorescence signal by using a Walz Imaging PAM System (M-series; Heinz Walz GmbH). To confirm the mutation of the target site, we further analyzed the putative mutants by using Sanger sequencing.

Genotype characterization

Genomic DNA was extracted as described in (Jeong *et al.*, 2018). For Sanger sequencing, the target regions were PCR-amplified by using specific primers (5′-GTAGTGTGCTTACATTTGCTGATT-3′ and 5′-CTACTGCTTCTGGATCTGTCC-3′ for the *lpa2* gene locus). The PCR products were separated by agarose gel electrophoresis, eluted from the gel, and sequenced (Macrogen). For targeted deep sequencing, genomic DNA segments that encompassed the nuclease target sites were amplified using Phusion polymerase (New England Biolabs). Equal amounts of PCR amplicons were subjected to paired-end read sequencing by using the Illumina MiSeq platform. The obtained next-generation sequencing data were analyzed using Cas-Analyzer (Park *et al.*, 2017). Reads that occurred only once were excluded to remove errors associated with amplification and sequencing. Insertions and deletions (indels) located around the Cas9 cleavage site (3 bp upstream of the protospacer–adjacent motif sequence) were considered to be induced mutations by Cas9. The targeted mutation efficiency was calculated from the mutation counts and the total counts of the reads. To examine the occurrence of potential off-target mutation sites, we used Cas-OFFinder (Bae *et al.*, 2014), which lists potential off-target sites with a DNA or RNA bulge in length that differ from the on-target sites by up to 4 nucleotides.

Pigment and cell size analysis

Pigment analyses were performed on cells grown in TAP medium at 70 μmol photons m^{-2} s^{-1} by HPLC, as described in (Lagarde *et al.*, 2000). Cell size was investigated using Countless® II FL automated cell counter (Themo Fisher).

Growth conditions

The *C. reinhardtii* strains were grown in minimal (HS) medium or in the presence of acetate (Tap medium; Kropat et al. 2011). Photoautotrophic and mixotrophic growth were evaluated in 80 mL photobioreactors in a Multi-cultivator system (Photon System Instruments, Cech Republic) by growing different strains in either HS or TAP medium in continuous light at 70 µmol photons m^{-2} s^{-1}. Heterotrophic growth was evaluated in cells grown in TAP medium in the dark. Growth curves were retrieved from optical density (OD) measurements at 720 nm automatically acquired from the Multi-cultivator system every 30 minutes. Doubling times were calculated from the exponential phase of the growth curve as described in (Harris, 2009). Spot test was performed spotting cells grown in TAP medium at 70 µmol $m^{-2}s^{-1}$ at exponential phase. In particular, $3x10^2$, $3x10^3$ and $3x10^4$ cells were spotted in TAP or HS medium with 1% agar added; plates were then exposed to 50, 100 or 300 µmol $m^{-2}s^{-1}$ for four or six days respectively for cells in TAP or HS media.

2D-Deriphat/SDS-PAGE electrophoresis and western blots

The 2D-Deriphat/SDS-PAGE analysis was performed as described in (Jeong *et al.*, 2018). Thylakoid membranes isolated according to (Ferrante *et al.*, 2012) from cells in exponential phase grown in TAP medium in continuous light at 70 µmol photons m^{-2} s^{-1}. Isolated thylakoids were solubilized at a Chl concentration of 0.5 mg/mL with *n*-dodecyl-α-D-maltoside (final concentration, 0.75% for both wild type and *lpa2*), incubated on ice for 10 min, and centrifuged at 20,000 ×*g* for 10 min to remove unsolubilized material. Thylakoid membrane proteins (25 µg Chl) were loaded in each lane. After separation, one-dimensional native Deriphat–PAGE strips were cut and soaked in SDS-PAGE stacking buffer containing 5 M urea twice for 25 min each. The proteins were then separated using SDS-PAGE (12% gel containing 2 M urea). The acrylamide gels were stained with Coomassie blue. Immunoblot analysis for profiling chloroplast proteins was performed cells in exponential phase grown in TAP medium in continuous light at 70 µmol photons m^{-2} s^{-1}, as described by (Jeong *et al.*, 2018). Antibodies were purchased from Agrisera (α-D1: AS05084; α-D2: AS06146, α-CP43: AS111787, α-CP47: AS04038, α-PsbO: AS06142-33, α-PsbP: AS06142-23, α-LHCB4: AS06117, α-LHCB5: AS09407, α-LHCBM5: AS09408, α-LHCSR3: AS142766, α-PsaA: AS09408, , α-PetA: AS01005, α-AtpB: AS05085-10, α-RbcL: AS03037) except for Lhca3 and Lhca4 antibodies which were provided by Prof. Hippler (Petroutsos *et al.*, 2011, Jeong *et al.*, 2018) and the LPA2 antibody. Polyclonal antibodies for LPA2 protein were raised against two peptides—CGFGSETAKQKEAEAEASTSKP and

EALEARIKSRRKGRVEPKVKVC (Abfontier, South Korea). In the case of α-LHCBM5 it is important to note that the antibody recognize not only LHCBM5, but all the different LHCBM subunits in *C. reinhardtii*, as previously described (Girolomoni *et al.*, 2017).

Photosynthetic activity analysis

Photosynthetic activity of WT and mutant strains was measured in cells at exponential growth phase grown in TAP medium in continuous light at 70 μmol photons m^{-2} s^{-1}. Before the measurements, cells were washed with HS medium and cultivated in photoautotrophy for 12 hours. The PSII activity was analyzed by conducting fluorescence measurements on whole cells by using a Dual-PAM 100 instrument (WALZ). In particular, φPSII, φNO, φNPQ, and NPQ were measured in dark adapted samples (1 hour) using different actinic lights from 0 to 1700 μmol photons m^{-2} s^{-1}. The 77K fluorescence emission spectra were acquired using a charge-coupled device spectrophotometer (JBeamBio), as previously described (Allorent *et al.*, 2013). State transitions were measured on whole cells induced to state 1 or 2, as described in (Fleischmann *et al.*, 1999): in brief, State 1 (S1) was induced by shaking vigorously cells in a low light (□5μmol m^2 s^{-1}) with 10μm of DCMU for at least 15 min to oxidize the plastoquinone pool while State 2 (S2) was induced by adding 250 μm sodium azide to inhibit mitochondrial respiration and to reduce the plastoquinone pool. The P700 activity was measured using the Dual-PAM 101 following the kinetics of transient absorption at 830 nm after exposure to actinic light. The maximum P700 activity was measured after a pulse of saturating light. Electrochromic shift measurements were performed using a Photosynq that set the actinic light at 500 μmol photons m^{-2} s^{-1}. Light-dependent O_2 evolution curves were measured using Clark electrode, as reported in (Perozeni *et al.*, 2019). Light dependent O_2 evolution was also measured at 600 μmol photons m^{-2} s^{-1} in presence of artificial PSII electron acceptor 2,6-Dichloro-1,4-benzoquinone (DCBQ) 0.25 mM, 1mM Potassium ferricyanide(III) and 1mM Dibromothymoquinone (DBMIB) (Brinkert *et al.*, 2016). PSII repair kinetics were measured after exposure to strong light (1800 μmol photons m^{-2} s^{-1}) until the Fv/Fm values were reduced to 0.05. PSII regeneration was then induced in low light (15 μmol photons m^{-2} s^{-1}) by measuring the Fv/Fm. The Fv/Fm values were measured after 3 min dark adaptation of whole cells.

Pulse-chase and immunoprecipitation

Immunoprecipitation experiments were performed in cells in exponential phase grown in TAP medium in continuous light at 70 μmol photons m^{-2} s^{-1} as described by (De Marchis *et al.*, 2018) for tobacco protoplasts, with minor modifications. In brief, approximately three million algae cells as sample were subjected to pulse-labelling up to 2 h by using Pro-Mix (a mixture of [^{35}S]Met and [^{35}S]Cys; GE Healthcare Little Chalfont, Buckinghamshire, United Kingdom). After the pulse, chase was performed by adding unlabeled Met and Cys to final concentrations of 10 and 5 mM, respectively. Cells were sampled at different pulse and chase time points. The cells were homogenized by adding homogenization buffer (150 mm Tris–Cl, pH 7.5; 150 mm NaCl; 1.5 mm EDTA; 2% Triton X-100; and Complete protease inhibitor cocktail [Roche]) to frozen samples. Proteins were immunoselected using rabbit polyclonal antisera against D2. The immunoprecipitates were analyzed using SDS-PAGE. After electrophoresis, gels were treated with AmplifyTM fluorography reagent (GE Healthcare), dried, and exposed for fluorography.

The *de novo* biosynthesis of D1 protein

To block the translation of the chloroplast-encoded D1 protein, we added lincomycin, an inhibitor of plastid protein biosynthesis, to the cultures, as described in (Jin *et al.*, 2003), and the cells were incubated in TAP medium under either normal growth light (50 μmol photons m^{-2} s^{-1}) or high light (500 μmol photons m^{-2} s^{-1}). Cells were harvested at 0, 30, 60, and 90 min after the light treatment, and the cell pellets were resuspended in Laemmli sample buffer (Laemmli, 1970) without bromophenol blue. After vigorous vortexing, the protein content of the crude extracts was measured using Bradford reagent (Bio-Rad).

RNA expression analysis

Total RNA was isolated from high light–treated cells in TAP medium by using an RNeasy Plant Mini Kit (Qiagen). Total RNA (1 μg) was used as a template for cDNA synthesis by using SuperScript III reverse transcriptase (ThermoFisher Scientific). Next, the cDNA was used as a template to amplify *PsbC* with real-time PCR by using SYBR Premix Ex Taq II (TaKaRa) and a Thermal Cycler Dice Real Time System (TaKaRa). The relative quantities of the transcript were normalized to those of the constitutively expressed *RACK1* gene. The following primer sequences used for the amplification: 5′-CAAGAACGTCGTGCTGCTGAA-3′ and 5′-CCTGCGTGCCATAAGTGACC-3′for ELIP2, (Cre09.g393173),5′-CAACTACAGCTGGGTGATCCT-3′ and 5′-AGTGTCCAGCTCCCTTTCAG-3′ for LPA2, and

5′-GGCTGGGACAAGATGGTCAA-3′ and 5′-GAGAAGCACAGGCAGTGGAT-3′ for RACK1(Cre06.g278222).

DATA AVAILABILITY STATEMENT

All the data herein described are included in Figures or in the Supporting Information. The strains here is investigated are fully available upon request to corresponding authors.

ACKNOWLEDGMENTS

This research was supported by Carbon to X Project" (2020M3H7A1098294) of the National Research Foundation (NRF) of Korea funded by the Korean government to EJ and by the ERC Starting Grant SOLENALGAE (679814) and FARE 2016-2017 grant (R16MHB7BMY) funded by the Italian ministry of education university and research (MIUR) to MB.

AUTHOR CONTRIBUTIONS

EJ and MB designed and moderated the research. SB coordinated the generation of the mutant strains. MC, JJ, MK, AP, WS, LZ, SC, SP, CB and SB performed experiments. MC, JJ, MB, and EJ drafted the manuscript. All the authors analyzed and contributed to data interpretation.

CONFLICT OF INTEREST STATEMENT

The authors declare that they have no competing interests.

SUPPORTING INFORMATION

Table S1. Accession numbers of LPA2 homologs used in the phylogenetic analysis.
Table S2. Target sequences of sgRNA used to recognize the *lpa2* gene.
Table S3. Mutation (insertion and deletion; indel) frequency of wild type and RGEN-transfected cells for each sgRNA.
Table S4. Analysis of off-target effects in the wild type and *lpa2* mutant.

Figure S1. Gene expression and localization of LPA2 in *C. reinhardtii*.

Figure S2. 77K fluorescence emission spectra of wild type (WT) and *lpa2* mutant.

Figure S3. Light intensity response curves of fluorescent photosynthetic parameters

Figure S4. Accumulation of photosynthetic proteins per cell in *lpa2* mutants

Figure S5. Time course analysis for the loss of the D1 protein after a low light to high light shift.

REFERENCES

Allorent, G., Tokutsu, R., Roach, T., Peers, G., Cardol, P., Girard-Bascou, J., Seigneurin-Berny, D., Petroutsos, D., Kuntz, M., Breyton, C., Franck, F., Wollman, F.A., Niyogi, K.K., Krieger-Liszkay, A., Minagawa, J. and Finazzi, G. (2013) A dual strategy to cope with high light in Chlamydomonas reinhardtii. ***Plant Cell*****, 25, 545-557.**

Armbruster, U., Zühlke, J., Rengstl, B., Kreller, R., Makarenko, E., Rühle, T., Schünemann, D., Jahns, P., Weisshaar, B. and Nickelsen, J. (2010) The Arabidopsis thylakoid protein PAM68 is required for efficient D1 biogenesis and photosystem II assembly. ***The plant cell*****, 22, 3439-3460.**

Bae, S., Park, J. and Kim, J.-S. (2014) Cas-OFFinder: a fast and versatile algorithm that searches for potential off-target sites of Cas9 RNA-guided endonucleases. ***Bioinformatics*****, 30, 1473-1475.**

Baek, K., Kim, D.H., Jeong, J., Sim, S.J., Melis, A., Kim, J.-S., Jin, E. and Bae, S. (2016) DNA-free two-gene knockout in Chlamydomonas reinhardtii via CRISPR-Cas9 ribonucleoproteins. ***Scientific Reports*****, 6, 30620.**

Boehm, M., Romero, E., Reisinger, V., Yu, J., Komenda, J., Eichacker, L.A., Dekker, J.P. and Nixon, P.J. (2011) Investigating the early stages of Photosystem II assembly in Synechocystis sp. PCC 6803 isolation of CP47 and CP43 complexes. ***Journal of Biological Chemistry*****, 286, 14812-14819.**

Bonente, G., Pippa, S., Castellano, S., Bassi, R. and Ballottari, M. (2012) Acclimation of Chlamydomonas reinhardtii to Different Growth Irradiances. ***Journal of Biological Chemistry*****, 287.**

Bricker, T.M., Roose, J.L., Fagerlund, R.D., Frankel, L.K. and Eaton-Rye, J.J. (2012) The extrinsic proteins of Photosystem II. *Biochimica et Biophysica Acta (BBA)-Bioenergetics*, 1817, 121-142.

Brinkert, K., Le Formal, F., Li, X., Durrant, J., Rutherford, A.W. and Fantuzzi, A. (2016) Photocurrents from photosystem II in a metal oxide hybrid system: Electron transfer pathways. *Biochim Biophys Acta*, 1857, 1497-1505.

Böhme, H. (1976) Photoreactions of cytochrome b6 and cytochrome f in chloroplast photosystem I fragments. *Z Naturforsch C*, 31, 68-77.

Cai, W., Ma, J., Chi, W., Zou, M., Guo, J., Lu, C. and Zhang, L. (2010) Cooperation of LPA3 and LPA2 is essential for photosystem II assembly in Arabidopsis. *Plant physiology*, 154, 109-120.

Cazzaniga, S., Kim, M., Bellamoli, F., Jeong, J., Lee, S., Perozeni, F., Pompa, A., Jin, E. and Ballottari, M. (2020) Photosystem II antenna complexes CP26 and CP29 are essential for nonphotochemical quenching in Chlamydomonas reinhardtii. *Plant Cell Environ*, 43, 496-509.

Chi, W., Ma, J. and Zhang, L. (2012) Regulatory factors for the assembly of thylakoid membrane protein complexes. *Philosophical Transactions of the Royal Society B: Biological Sciences*, 367, 3420-3429.

De Marchis, F., Colanero, S., Klein, E.M., Mainieri, D., Prota, V.M., Bellucci, M., Pagliuca, G., Zironi, E., Gazzotti, T. and Vitale, A. (2018) Expression of CLAVATA3 fusions indicates rapid intracellular processing and a role of ERAD. *Plant Science*, 271, 67-80.

Dinc, E., Tian, L., Roy, L.M., Roth, R., Goodenough, U. and Croce, R. (2016) LHCSR1 induces a fast and reversible pH-dependent fluorescence quenching in LHCII in Chlamydomonas reinhardtii cells. *Proc Natl Acad Sci U S A*, 113, 7673-7678.

Edgar, R.C. (2004) MUSCLE: multiple sequence alignment with high accuracy and high throughput. ***Nucleic acids research*****, 32, 1792-1797.**

Ferrante, P., Ballottari, M., Bonente, G., Giuliano, G. and Bassi, R. (2012) LHCBM1 and LHCBM2/7 polypeptides, components of major LHCII complex, have distinct functional roles in photosynthetic antenna system of Chlamydomonas reinhardtii. ***Journal of biological chemistry*****, 287, 16276-16288.**

Fleischmann, M.M., Ravanel, S., Delosme, R., Olive, J., Zito, F., Wollman, F.-A. and Rochaix, J.-D. (1999) Isolation and Characterization of Photoautotrophic Mutants ofChlamydomonas reinhardtii Deficient in State Transition. ***Journal of Biological Chemistry*****, 274, 30987-30994.**

Fu, A., He, Z., Cho, H.S., Lima, A., Buchanan, B.B. and Luan, S. (2007) A chloroplast cyclophilin functions in the assembly and maintenance of photosystem II in Arabidopsis thaliana. ***Proc Natl Acad Sci U S A*****, 104, 15947-15952.**

Girolomoni, L., Cazzaniga, S., Pinnola, A., Perozeni, F., Ballottari, M. and Bassi, R. (2019) LHCSR3 is a nonphotochemical quencher of both photosystems in Chlamydomonas reinhardtii. ***Proceedings of the National Academy of Sciences of the United States of America*****, 116, 4212-4217.**

Girolomoni, L., Ferrante, P., Berteotti, S., Giuliano, G., Bassi, R. and Ballottari, M. (2017) The function of LHCBM4/6/8 antenna proteins in Chlamydomonas reinhardtii. ***J Exp Bot*****, 68, 627-641.**

Gokhale, Z. and Sayre, R.T. (2009) Photosystem II, a structural perspective. In ***The Chlamydomonas Sourcebook*****: Elsevier, pp. 573-602.**

Guindon, S., Dufayard, J.F., Lefort, V., Anisimova, M., Hordijk, W. and Gascuel, O. (2010) New algorithms and methods to estimate maximum-likelihood phylogenies: assessing the performance of PhyML 3.0. ***Syst Biol*****, 59, 307-321.**

Harris, E.H. (2009) ***The Chlamydomonas sourcebook. Introduction to Chlamydomonas and its laboratory use*** **2 edn. Amsterdam, The Netherlands: Elsevier.**

Jeong, J., Baek, K., Kirst, H., Melis, A. and Jin, E. (2017) Loss of CpSRP54 function leads to a truncated light-harvesting antenna size in Chlamydomonas reinhardtii. ***Biochimica et Biophysica Acta (BBA)-Bioenergetics*****, 1858, 45-55.**

Jeong, J., Baek, K., Yu, J., Kirst, H., Betterle, N., Shin, W., Bae, S., Melis, A. and Jin, E. (2018) Deletion of the chloroplast LTD protein impedes LHCI import and PSI–LHCI assembly in Chlamydomonas reinhardtii. ***Journal of experimental botany*****, 69, 1147-1158.**

Jin, E., Yokthongwattana, K., Polle, J.E. and Melis, A. (2003) Role of the reversible xanthophyll cycle in the photosystem II damage and repair cycle in Dunaliella salina. ***Plant Physiol*****, 132, 352-364.**

Järvi, S., Suorsa, M. and Aro, E.-M. (2015) Photosystem II repair in plant chloroplasts—regulation, assisting proteins and shared components with photosystem II biogenesis. ***Biochimica et Biophysica Acta (BBA)-Bioenergetics*****, 1847, 900-909.**

Kirst, H. and Melis, A. (2014) The chloroplast signal recognition particle (CpSRP) pathway as a tool to minimize chlorophyll antenna size and maximize photosynthetic productivity. ***Biotechnology advances*****, 32, 66-72.**

Komenda, J., Knoppová, J., Kopečná, J., Sobotka, R., Halada, P., Yu, J., Nickelsen, J., Boehm, M. and Nixon, P.J. (2012) The Psb27 assembly factor binds to the CP43 complex of photosystem II in the cyanobacterium Synechocystis sp. PCC 6803. ***Plant physiology*****, 158, 476-486.**

Kosuge, K., Tokutsu, R., Kim, E., Akimoto, S., Yokono, M., Ueno, Y. and Minagawa, J. (2018) LHCSR1-dependent fluorescence quenching is mediated by excitation energy transfer from LHCII to photosystem I in. ***Proc Natl Acad Sci U S A*****, 115, 3722-3727.**

Laemmli, U.K. (1970) Cleavage of structural proteins during the assembly of the head of bacteriophage T4. ***Nature*****, 227, 680-685.**

Lagarde, D., Beuf, L. and Vermaas, W. (2000) Increased production of zeaxanthin and other pigments by application of genetic engineering techniques toSynechocystis sp. strain PCC 6803. *Appl. Environ. Microbiol.*, 66, 64-72.

Lefort, V., Longueville, J.E. and Gascuel, O. (2017) SMS: Smart Model Selection in PhyML. *Mol Biol Evol*, 34, 2422-2424.

Lu, Y. (2016) Identification and roles of photosystem II assembly, stability, and repair factors in Arabidopsis. *Frontiers in plant science*, 7, 168.

Ma, J., Peng, L., Guo, J., Lu, Q., Lu, C. and Zhang, L. (2007) LPA2 is required for efficient assembly of photosystem II in Arabidopsis thaliana. *Plant Cell*, 19, 1980-1993.

Marín-Navarro, J., Manuell, A.L., Wu, J. and Mayfield, S.P. (2007) Chloroplast translation regulation. *Photosynthesis Research*, 94, 359-374.

Melis, A. (1999) Photosystem-II damage and repair cycle in chloroplasts: what modulates the rate of photodamage in vivo? *Trends in plant science*, 4, 130-135.

Nelson, N. and Junge, W. (2015) Structure and energy transfer in photosystems of oxygenic photosynthesis. *Annual review of biochemistry*, 84, 659-683.

Nickelsen, J. and Rengstl, B. (2013) Photosystem II assembly: from cyanobacteria to plants. *Annual review of plant biology*, 64, 609-635.

Park, J., Lim, K., Kim, J.-S. and Bae, S. (2017) Cas-analyzer: an online tool for assessing genome editing results using NGS data. *Bioinformatics*, 33, 286-288.

Peers, G., Truong, T.B., Ostendorf, E., Busch, A., Elrad, D., Grossman, A.R., Hippler, M. and Niyogi, K.K. (2009) An ancient light-harvesting protein is critical for the regulation of algal photosynthesis. *Nature*, 462, 518-521.

Perozeni, F., Cazzaniga, S. and Ballottari, M. (2019) In vitro and in vivo investigation of chlorophyll binding sites involved in non-photochemical quenching in Chlamydomonas reinhardtii. *Plant, cell & environment*, 42, 2522-2535.

Petroutsos, D., Busch, A., Janssen, I., Trompelt, K., Bergner, S.V., Weinl, S., Holtkamp, M., Karst, U., Kudla, J. and Hippler, M. (2011) The chloroplast calcium sensor CAS is required for photoacclimation in Chlamydomonas reinhardtii. *Plant Cell*, 23, 2950-2963.

Potter, S.C., Luciani, A., Eddy, S.R., Park, Y., Lopez, R. and Finn, R.D. (2018) HMMER web server: 2018 update. *Nucleic Acids Res*, 46, W200-W204.

Rokka, A., Suorsa, M., Saleem, A., Battchikova, N. and Aro, E.M. (2005) Synthesis and assembly of thylakoid protein complexes: multiple assembly steps of photosystem II. *Biochem J*, 388, 159-168.

Schneider, A., Steinberger, I., Strissel, H., Kunz, H.H., Manavski, N., Meurer, J., Burkhard, G., Jarzombski, S., Schünemann, D., Geimer, S., Flügge, U.I. and Leister, D. (2014) The Arabidopsis Tellurite resistance C protein together with ALB3 is involved in photosystem II protein synthesis. *Plant J*, 78, 344-356.

Shen, L., Huang, Z., Chang, S., Wang, W., Wang, J., Kuang, T., Han, G., Shen, J.R. and Zhang, X. (2019) Structure of a $C_2S_2M_2N_2$-type PSII-LHCII supercomplex from the green alga *Chlamydomonas reinhardtii*. *Proc Natl Acad Sci U S A*, 116, 21246-21255.

Shinozaki, K., Ohme, M., Tanaka, M., Wakasugi, T., Hayashida, N., Matsubayashi, T., Zaita, N., Chunwongse, J., Obokata, J., Yamaguchi-Shinozaki, K., Ohto, C., Torazawa, K., Meng, B.Y., Sugita, M., Deno, H., Kamogashira, T., Yamada, K., Kusuda, J., Takaiwa, F., Kato, A., Tohdoh, N., Shimada, H. and Sugiura, M. (1986) The complete nucleotide sequence of the tobacco chloroplast genome: its gene organization and expression. *EMBO J*, 5, 2043-2049.

Snellenburg, J.J., Wlodarczyk, L.M., Dekker, J.P., van Grondelle, R. and van Stokkum, I.H. (2017) A model for the 77K excited state dynamics in Chlamydomonas reinhardtii in state 1 and state 2. *Biochim Biophys Acta*, 1858, 64-72.

Spaniol, B., Lang, J., Venn, B., Schake, L., Sommer, F., Mustas, M., Wollman, F.-A., Choquet, Y., Mühlhaus, T. and Schroda, M. (2021) Complexome profiling on the lpa2 mutant reveals

insights into PSII biogenesis and new PSII associated proteins. *bioRxiv*, 2021.2001.2004.425283.

Su, X., Ma, J., Wei, X., Cao, P., Zhu, D., Chang, W., Liu, Z., Zhang, X. and Li, M. (2017) Structure and assembly mechanism of plant C2S2M2-type PSII-LHCII supercomplex. *Science*, 357, 815-820.

Tang, J.X., Chen, D., Deng, S.L., Li, J., Li, Y., Fu, Z., Wang, X.X., Zhang, Y., Chen, S.R. and Liu, Y.X. (2018) CRISPR/Cas9-mediated genome editing induces gene knockdown by altering the pre-mRNA splicing in mice. *BMC Biotechnol*, 18, 61.

Tuladhar, R., Yeu, Y., Tyler Piazza, J., Tan, Z., Rene Clemenceau, J., Wu, X., Barrett, Q., Herbert, J., Mathews, D.H., Kim, J., Hyun Hwang, T. and Lum, L. (2019) CRISPR-Cas9-based mutagenesis frequently provokes on-target mRNA misregulation. *Nat Commun*, 10, 4056.

Uniacke, J. and Zerges, W. (2007) Photosystem II assembly and repair are differentially localized in Chlamydomonas. *Plant Cell*, 19, 3640-3654.

van Amerongen, H. and Croce, R. (2013) Light harvesting in photosystem II. *Photosynth Res*, 116, 251-263.

Wang, P., Liu, J., Liu, B., Feng, D., Da, Q., Shu, S., Su, J., Zhang, Y., Wang, J. and Wang, H.-B. (2013) Evidence for a role of chloroplastic m-type thioredoxins in the biogenesis of photosystem II in Arabidopsis. *Plant physiology*, 163, 1710-1728.

Wei, L., Guo, J., Ouyang, M., Sun, X., Ma, J., Chi, W., Lu, C. and Zhang, L. (2010) LPA19, a Psb27 homolog in Arabidopsis thaliana, facilitates D1 protein precursor processing during PSII biogenesis. *Journal of Biological Chemistry*, 285, 21391-21398.

Whelan, S. and Goldman, N. (2001) A general empirical model of protein evolution derived from multiple protein families using a maximum-likelihood approach. *Mol Biol Evol*, 18, 691-699.

Zerges, W., Auchincloss, A.H. and Rochaix, J.-D. (2003) Multiple translational control sequences in the 5′ leader of the chloroplast psbC mRNA interact with nuclear gene products in Chlamydomonas reinhardtii. *Genetics*, 163, 895-904.

Zhang, D., Zhou, G., Liu, B., Kong, Y., Chen, N., Qiu, Q., Yin, H., An, J., Zhang, F. and Chen, F. (2011) HCF243 encodes a chloroplast-localized protein involved in the D1 protein stability of the Arabidopsis photosystem II complex. *Plant physiology*, 157, 608-619.

Zhang, S., Frankel, L.K. and Bricker, T.M. (2010) The Sll0606 protein is required for photosystem II assembly/stability in the cyanobacterium Synechocystis sp. PCC 6803. *Journal of Biological Chemistry*, 285, 32047-32054.

Ziehe, D., Dünschede, B. and Schünemann, D. (2017) From bacteria to chloroplasts: evolution of the chloroplast SRP system. *Biological chemistry*, 398, 653-661.

FIGURE/TABLE LEGENDS

Figure 1. Maximum-likelihood tree (**A**) and amino acid sequence alignment (**B**) of LPA2 homologs in the green lineage. The sequences were aligned using MUSCLE alignment, and selected species representing each clade are shown in **B**. Node labels are bootstrap support values from 100 replicates. The species names and accession number of individual sequences are labeled in the tip of the branch. Green closed triangle represents the the Cas9 driven mutation site of LPA2 gene in *lpa2*.

Figure 2. CRISPR-Cas9-mediated *lpa2* mutants generation in *C. reinhardtii*. **A**. The measurement of F_v/F_m to select putative *LPA2* gene knockout mutants grown on TAP agar medium under 50 μmol photons m^{-2} s^{-1}. The cells (marked with white arrows) presenting lower F_v/F_m than the background cells were picked and confirmed by Sanger sequencing. **B**. DNA sequence alignment of the wild-type (WT) and *lpa2* mutants obtained from Figure 2A at the *LPA2* locus. The 20-bp target sequence of sgRNA2 is underlined, and the PAM sequence is shown in blue. The column on

the right indicates the number of inserted (+) or deleted (−) bases. C. Relative mRNA expression of the LPA2 gene in *lpa2* mutants compared to the WT case. mRNA expression level were calculated based on the WT upon normalization with the expression level of the RACK1 gene, used as internal standard. Error bars are reported as standard deviation (n=3). D. **D**. Immunoblot with LPA2 and AtpB (loading control) antibodies in the WT and *lpa2* 1# and *lpa2* #2, which were used for all further experiments. Proteins were loaded on the basis of equal cell numbers, and the WT samples were loaded at three different concentrations (25%, 50%, and 100%). **E**. The measurement of Chl fluorescence kinetics in the WT and *lpa2* mutants grown in liquid TAP medium under 50 µmol photons m^{-2} s^{-1}. The measuring light (ML) and saturating light (SL) were 5 and 1,250 µmol photons m^{-2} s^{-1}, respectively. The F_v/F_m differed significantly between the WT and *lpa2* mutants, as determined by Student *t*-test (n = 4; the values shown are means ± SD; $p < 0.05$).

Figure 3. Growth curves of WT and *lpa2* mutants. Heterotrophic (**A**), photoautotrophic (**B**), and mixotrophic (**C**) growth of the *lpa2* mutants measured in liquid medium and compared to the wild type (WT). Heterotrophic conditions were induced growing microalgae strains in the dark in TAP medium, while photoautotrophic and mixotrophic conditions were obtained growing the cells in continuous light respectively in HS or TAP media. Growth curves are reported as optical density (OD) measured at 720 nm every 30 minutes. The growth curves obtained were fitted using sigmoidal function (n = 4). Doubling time of cells in the different growth conditions are reported in Table 2. Photoautrophic and mixotrophic growth was also evaluated by spot test in solid HS or TAP media at 50, 100 and 300 µmol photons m^{-2} s^{-1} (**D**). The number of cells spotted for each drops are reported on the right of the Panel D.

Figure 4. Oxygen evolution curves of WT and *lpa2* mutants. Oxygen evolution rates of both the WT and *lpa2* mutants in response to different light intensities were measured to determine the rate of oxygen consumption in the dark. Cells were grown in TAP medium, washed with HS medium, and cultivated in photoautotrophy for 12 h prior to measurement. The net oxygen evolution rates were measured on samples at the same cell concentration (**A)**). Oxygen evolution was also measured at 600 µmol photons m^{-2} s^{-1} in presence of PSII electron acceptors DCBQ and Potassium ferrocyanide and DMBIB as inhibitor of plastoquinone reduction by cyclic electron flow: the net oxygen evolution rates were normalized to total cell contents (**B)**. Oxygen evolution

rates produced by WT and *lpa2* mutants in presence of DCBQ, Potassium ferrocyanide and DBMIB were then plotted as a function of D1 or D2 content per Chl (**C, D**). Error bars indicate standard deviation (n = 3). The statistical significance of differences between WT and *lpa2* is indicated as * $p < 0.05$, as determined by Student *t*-test. Results of linear fit of data reported in Panel C and D are reported as dashed line (R^2=0.926 and R^2= 0.99545 respectively for linear fits in Panel C and D).

Figure 5. PSI activity, ECS and state transitions. (A, B) Maximal P700 oxidation on a Chl (A) or cell (B) basis in the WT and *lpa2* mutants. (C). Linear electron flow (LEF) and cyclic electron flow (CEF) of the WT and *lpa2*#1 and *lpa2#2* estimated from the electrochromic shift (ECS) on a Chl basis. (D, E) State transitions analysis by using 77K fluorescence emission spectra of the wild type (WT; D) and *lpa2* #1 and *lpa2#2* mutants (E) in state 1 (S1) or state 2 (S2) conditions. (F) Maximum level of state transition measured as percentage variation of PSII fluorescence in S2 compared to S1. Error bars are indicated as standard deviation (n = 3). The statistical significance of differences between WT and *lpa2* mutants ($p < 0.01$) is indicated as *, as determined by Student *t*-test.

Figure 6. The 2D-Deriphat/SDS-PAGE of purified thylakoid membranes. Deriphat-PAGE of WT and *lpa2* mutants (**A**): density of each band was quantified by densitometric analysis of the green channel of the picture. Band marked with PSI core* is related to PSI-core with residual Lhca antenna bound. Second dimension of the 2D-Deriphat/SDS-PAGE was performed by running the Deriphat-PAGE lanes in Tris-Tricine poly-acrylamide gel. The statistical significance of differences between WT and *lpa2* is indicated as * $p < 0.05$, as determined by Student *t*-test (n=3). (**B**): Western blot analysis on 2D-Deriphat/SDS-PAGE by using specific antibodies recognizing D1, D2, CP43 or CP47 subunits is reported in (**C**).

Figure 7. Immunoblot analysis (**A, B**,) and Coomassie blue-stained SDS-PAGE gel (**C**) and of chloroplast proteins from the wild type (WT) and *lpa2* mutants. Results from immunoblotting with antibodies against PSII-LHCII are shown in **A** where specific antibodies recognizing the PSII core subunits D1, D2, CP4, CP47, PsbO and PsbP and the LHCII antenna complexes LHCB4 (CP29), LHCB5 (CP26) and LHCBM were used. For the latter in particular, the antibody LHCBM5 was

adopted which was reported to recognize all the different LHCBM subunits. Results from immunoblotting with antibodies against PSI core (α-PsaA), LHCI antenna (α-LHCA3, α-LHCA4), Cyt *f* (α-PetA), chloroplast ATPase β-subunit (α-AtpB), Large subunit of RUBISCO (α-RbcL) and LHCSR3 are shown in **B**. Each lane was loaded on a per Chl basis (1 μg), and the WT samples were loaded at three different concentrations (0.25, 0.5, and 1 μg). The amounts of proteins in the *lpa2#1* and lpa2#2 mutants compared to the WT are presented next to the protein bands expressed as percentage of WT level ($n \geq 3$; the values shown are means ± SD). The statistical significance of differences between WT and *lpa2* is indicated as * $p < 0.05$ and ** $p < 0.01$, as determined by Student *t*-test. In Panel **D** the protein content of D1, D2, CP43 CP47, PsaA, PetA, AtpB and RUBISCO were also reported normalized to D2 content, with the different ratios set as 1 in the case of WT (black line). (**E**) autoradiography of immunoprecipitated PSII complexes. *C. reinhardtii* WT and *lpa2* mutants' cells were grown in TAP medium at low light (70μmol $m^{-2}s^{-1}$) in presence of [^{35}S] methionine and [^{35}S] cysteine at different timing (pulses) indicated on top of the figure in minutes. PSII core complexes were extracted from thylakoid membranes by membrane solubilization and immunoprecipitation using D2 antibody. Chase experiments were performed after 60 minutes of pulse removing the labelled amino acids from the growth medium. The bands corresponding to D1/D2 and CP43/CP47 were identified according to their migration pattern, as reported in Panel **F** where immunoblotting results obtained on thylakoids membranes isolated from WT and loaded on the same SDS-PAGE gel system as in the case of **E**.

Figure 8. Kinetics of PSII activity photoinhibition and repair. Kinetics of PSII photoinhibition (A) and repair (B) was measured following the changes in maximum quantum yield (Fv/Fm) after exposure to strong light (1800 μmol m^{-2} s^{-1}). Panel A: kinetics of PSII activity (Fv/Fm) photoinhibition. Panel B: kinetics of Fv/Fm recovery in low light (15 μmol m^{-2} s^{-1}) after exposure to strong light (1800 μmol m^{-2} s^{-1}) for 15 minutes in the case of *lpa2* mutants and 25 minutes in the case of WT. Error bars are indicated as standard deviation (n = 3). The statistical significance of differences between WT and *lpa2* mutants ($p < 0.05$) is indicated as *, as determined by Student *t*-test.

Table1. Chlorophyll (Chl) content and cell diameter of the wild type (WT) and *lpa2* mutants. The statistical significance of differences between WT and *lpa2* mutants ($p < 0.05$, n=4) is indicated as *, as determined by Student *t*-test.

Table 2. Doubling times of WT and lpa2 mutant strains. Doubling times (h) for WT and lpa2 mutant were calculated for cells in exponential phase in mixotrophic, photoautotrophic and heterotrophic growth conditions as reported in Figure 3. The statistical significance of differences between WT and *lpa2* mutants ($p < 0.05$, n=3) is indicated as *, as determined by Student *t*-test.

TABLES

Table1. Chlorophyll (Chl) content and cell diameter of the wild type (WT) and *lpa2* mutants. The statistical significance of differences between WT and *lpa2* mutants ($p < 0.05$, n=4) is indicated as *, as determined by Student *t*-test.

	Chl/cell (pg/cell)	Chl a/b ratio	Chl/car	Cell diameter (µm)
WT	2.50 ± 0.11	2.61 ± 0.01	3.20 ± 0.03	8.92 ± 0.81
***lpa2* #1**	1.35 ± 0.11*	2.58 ± 0.02	2.70 ± 0.07*	8.57 ± 0.96

***lpa2* #2**	1.17 ± 0.05*	2.47 ± 0.07	2.82 ± 0.08*	8.39 ± 0.75

Table 2. Doubling times of WT and lpa2 mutant strains. Doubling times (h) for WT and lpa2 mutant were calculated for cells in exponential phase in mixotrophic, photoautotrophic and heterotrophic growth conditions as reported in Figure 3. The statistical significance of differences between WT and *lpa2* mutants ($p < 0.05$, n=3) is indicated as *, as determined by Student *t*-test.

	mixotrophy	**autotrophy**	**heterotrophy**
	TAP + LIGHT	**HS + LIGHT**	**TAP + DARK**
WT	7.8 ± 0.4	19.4 ± 0.3	18.3 ± 1.0
lpa2#1	14.6 ± 0.7*	388.3 ± 8.7*	15.4 ± 1.5
lpa2#2	11.8 ± 1.1*	406.5 ± 9.1*	18.3 ± 1.5

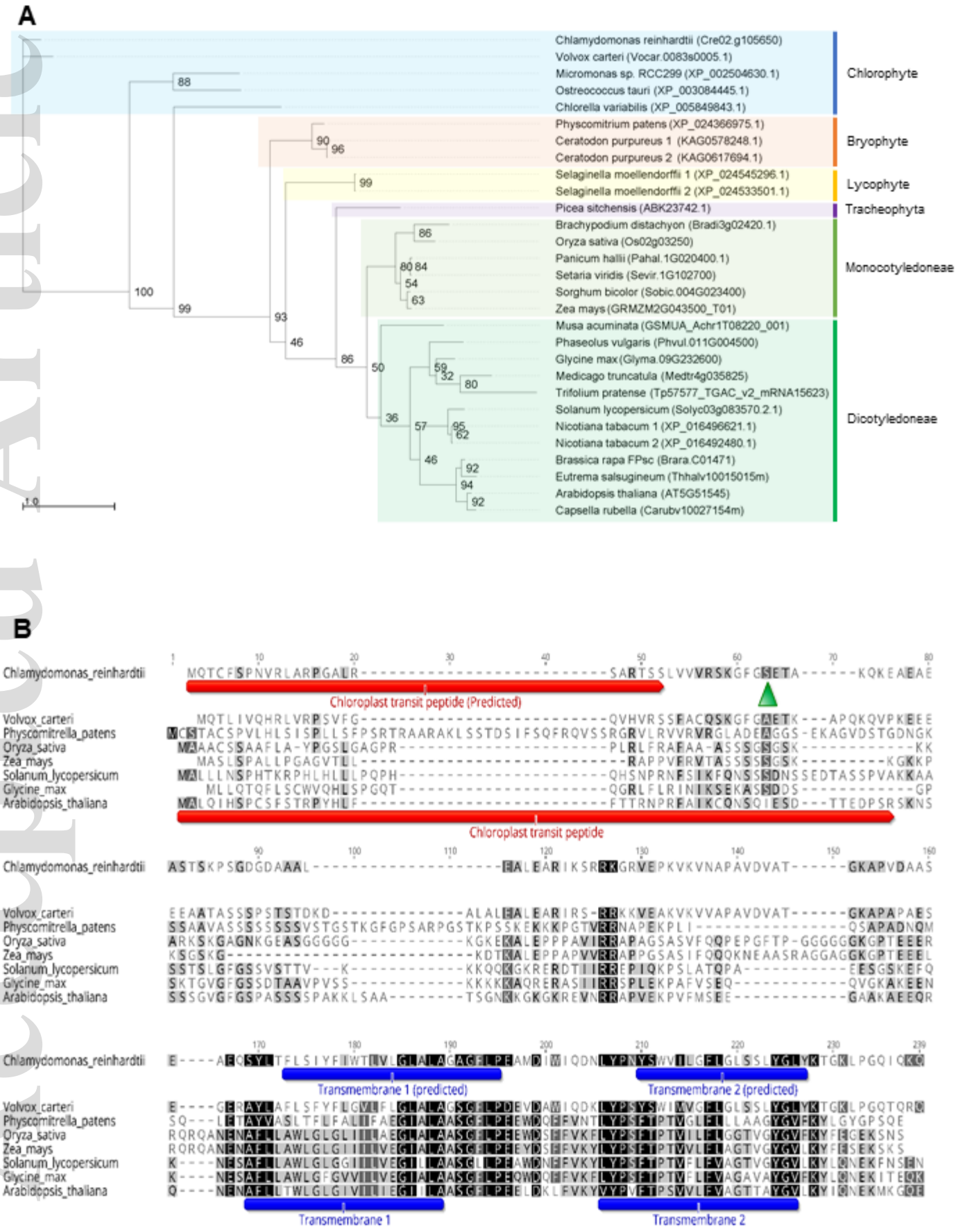

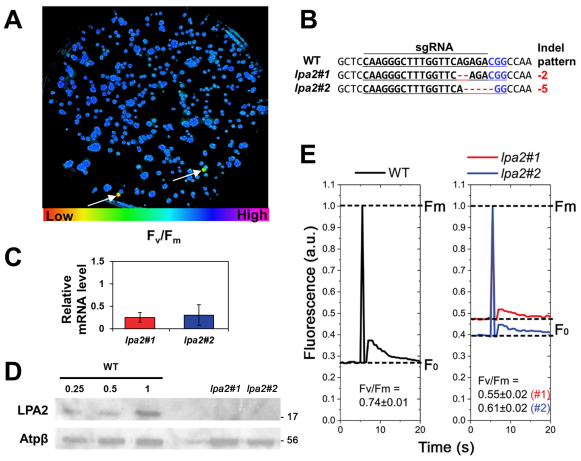

tpj_15405_f2.tif

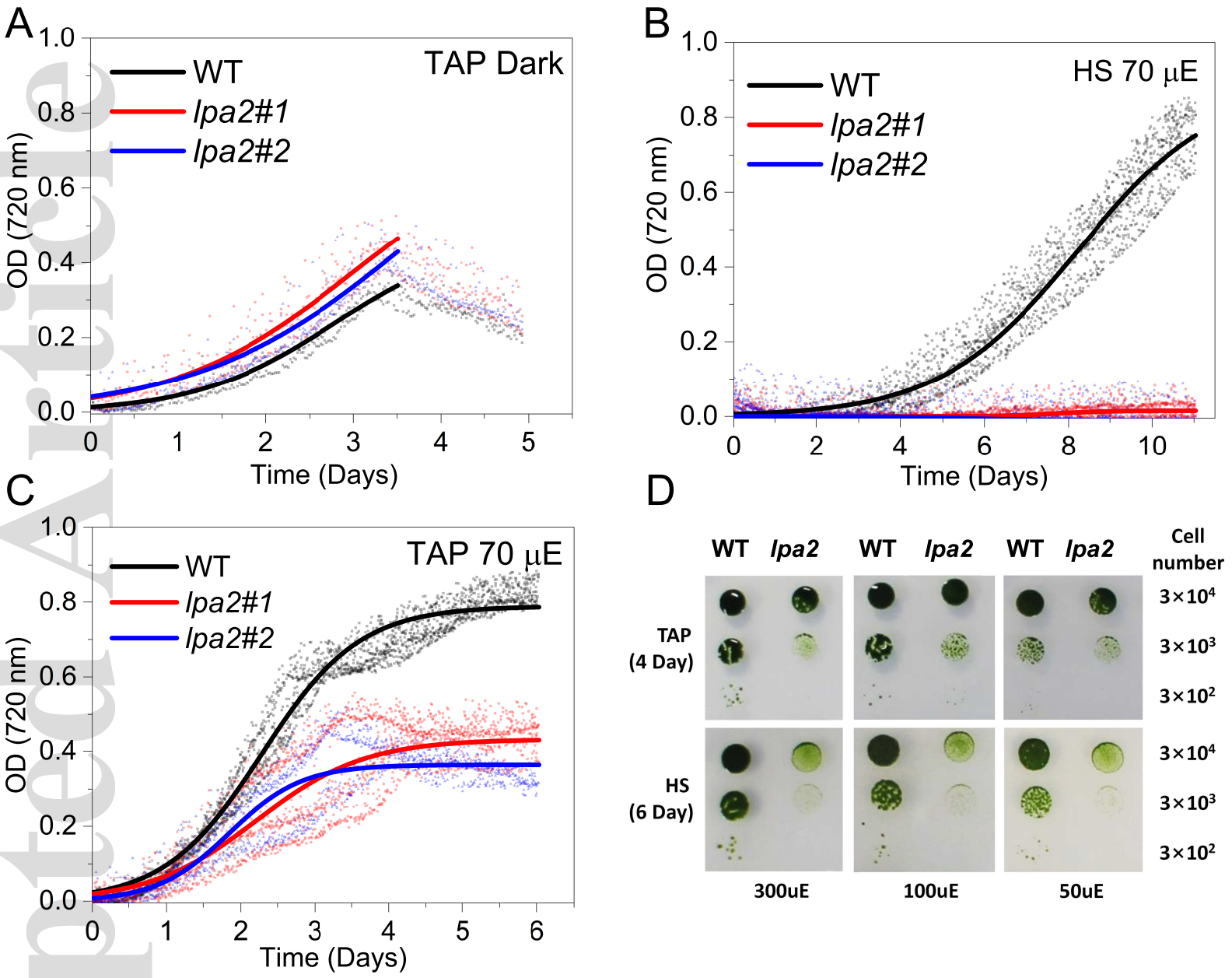

tpj_15405_f3.eps

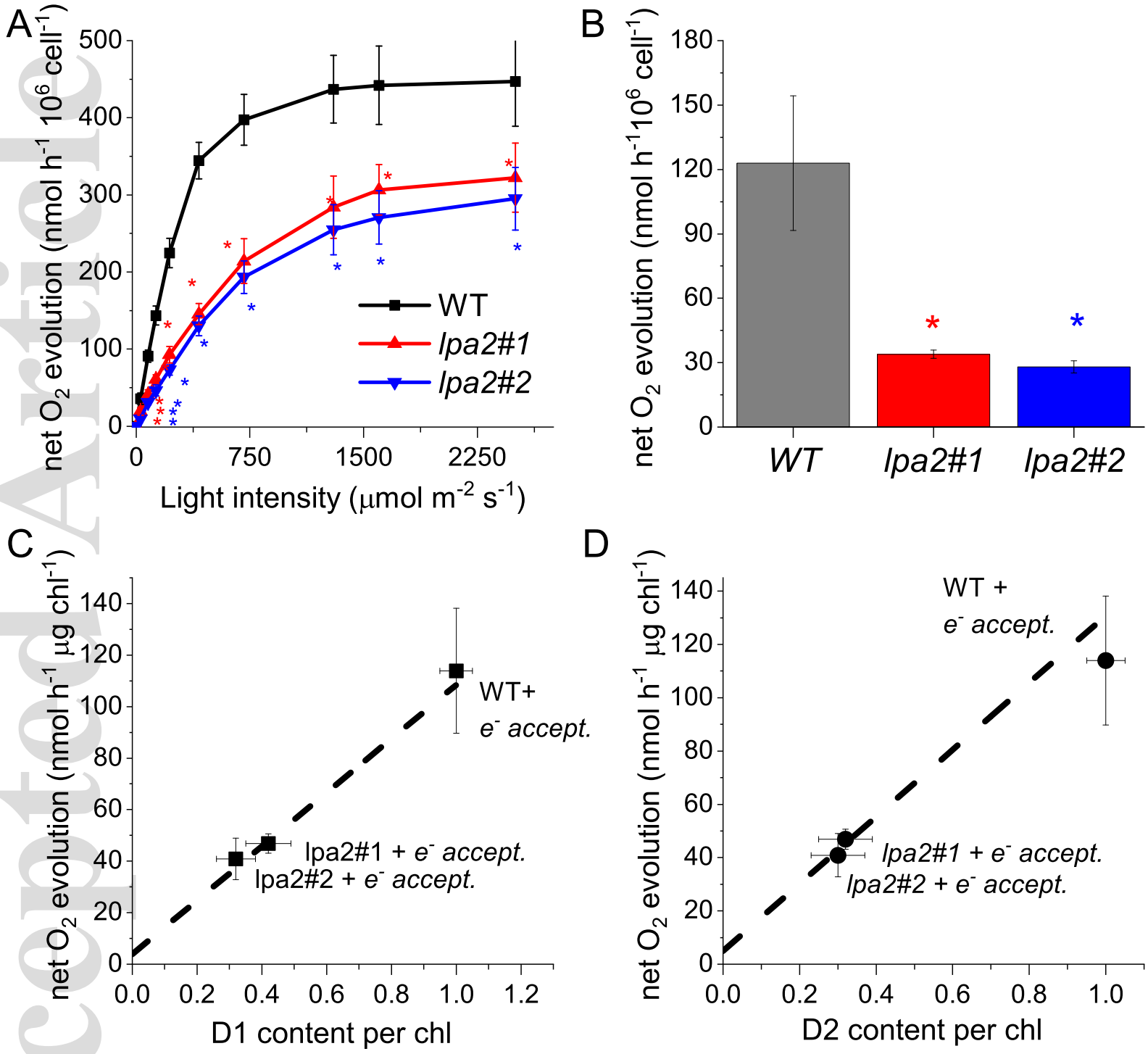

tpj_15405_f4.eps

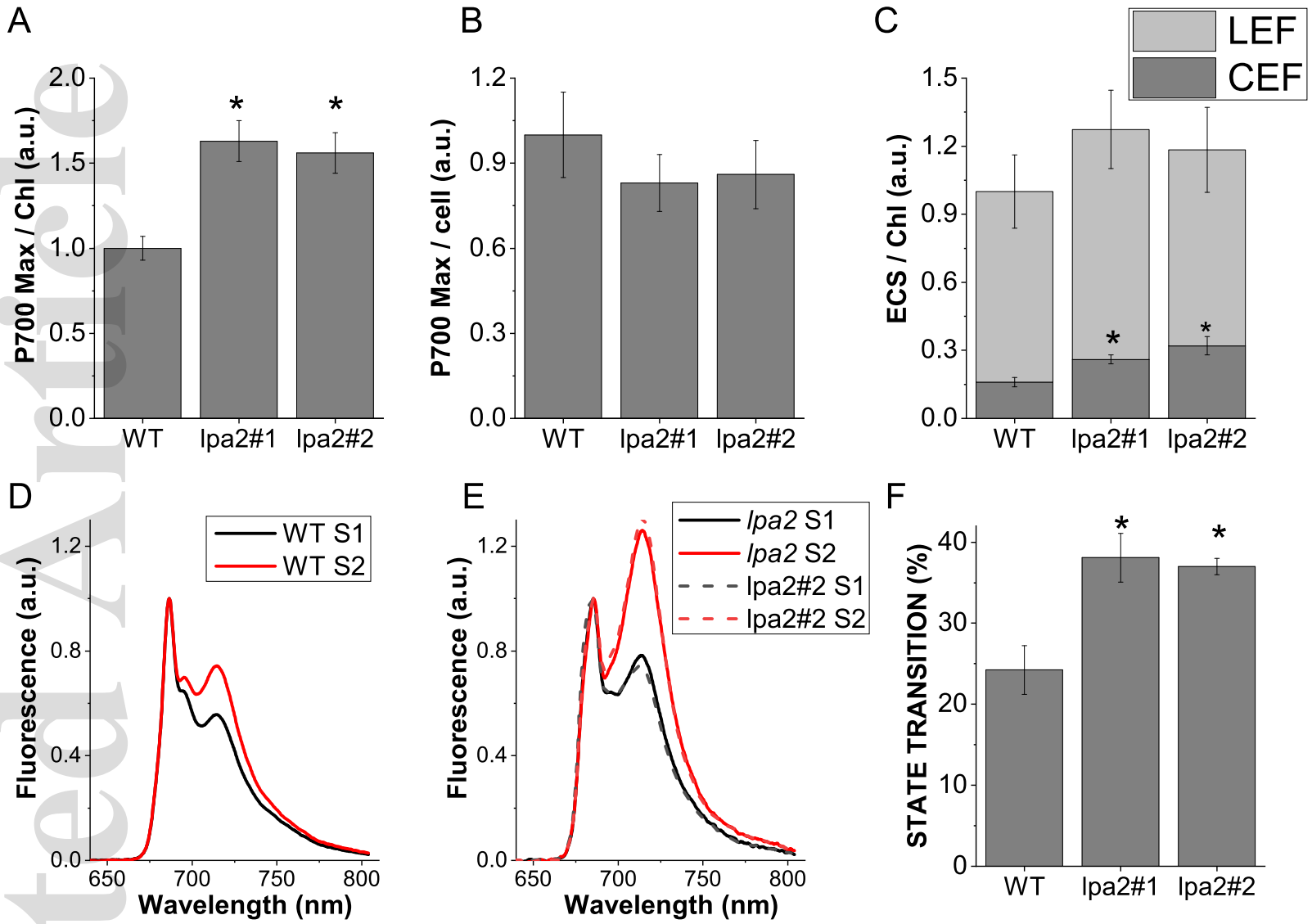

tpj_15405_f5.eps

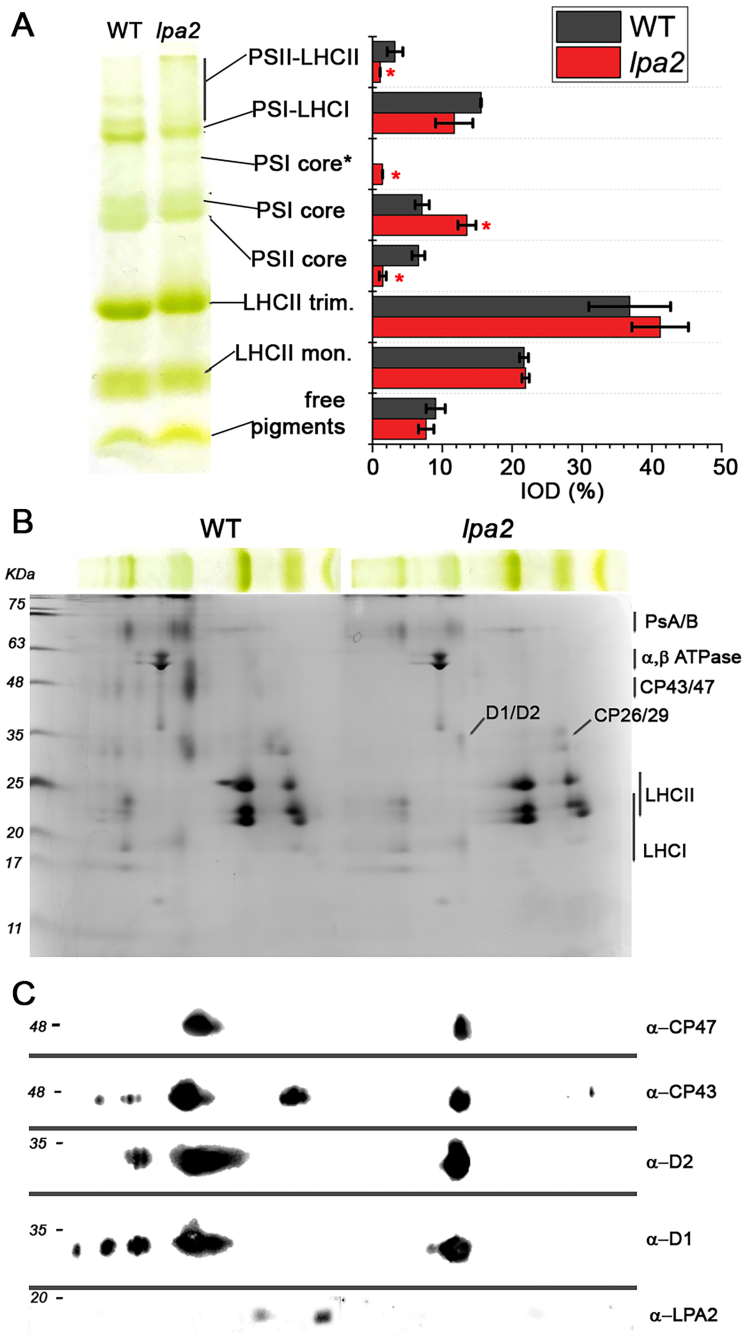

tpj_15405_f6.tif

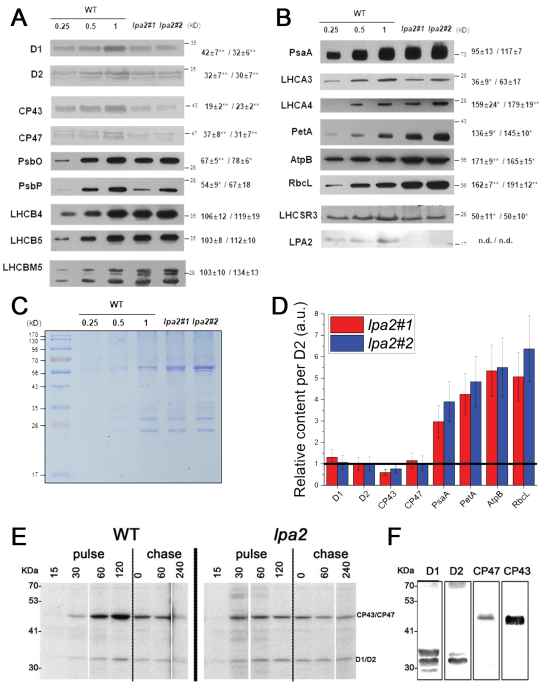

tpj_15405_f7.tif

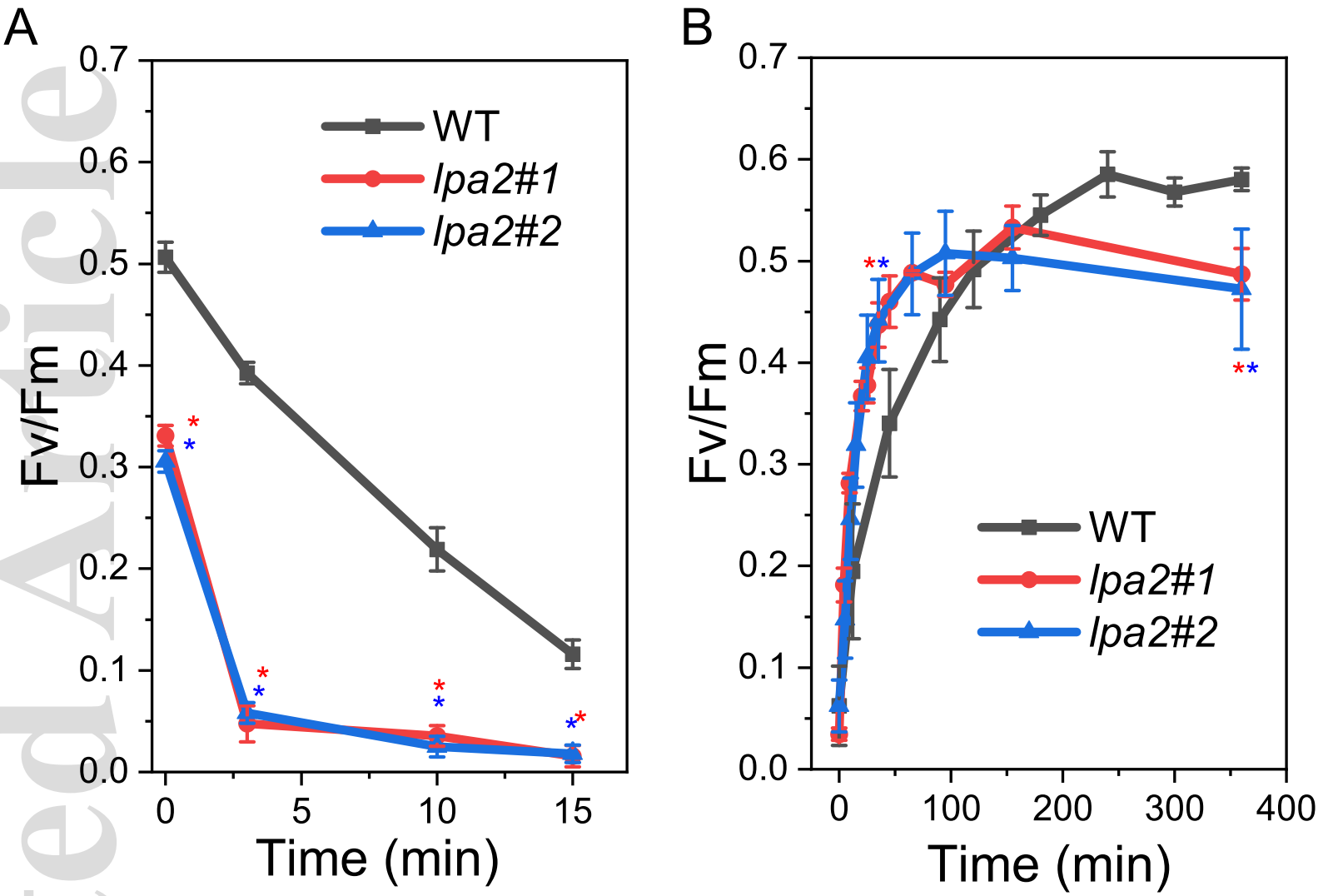

tpj_15405_f8.eps